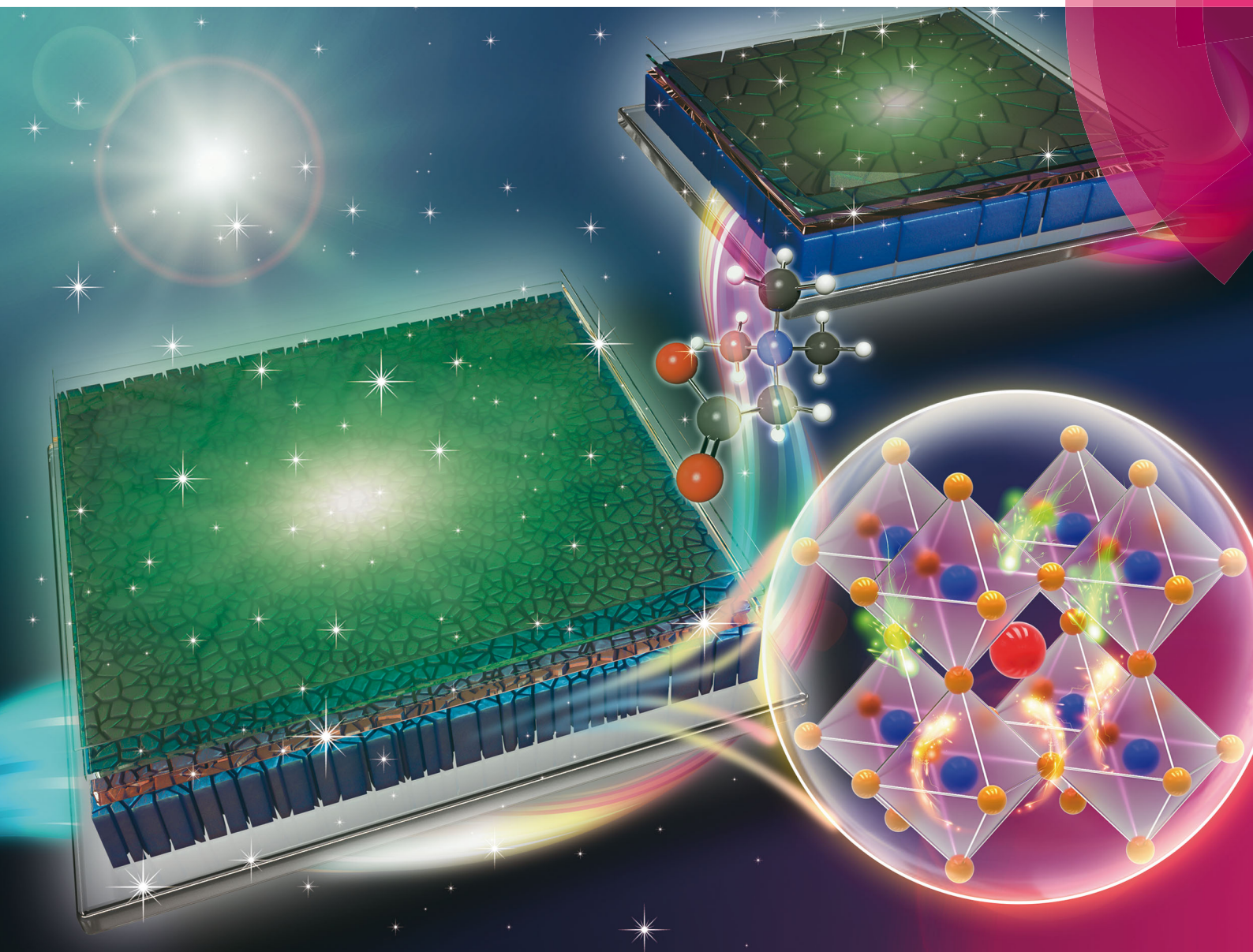


Journal of Materials Chemistry C

Materials for optical, magnetic and electronic devices

rsc.li/materials-c



ISSN 2050-7526



ROYAL SOCIETY
OF CHEMISTRY

Celebrating
IYPT 2019

PAPER

Man-Keung Fung *et al.*

Interfacial engineering for highly efficient quasi-two dimensional organic–inorganic hybrid perovskite light-emitting diodes

Cite this: *J. Mater. Chem. C*, 2019,
7, 4344

Interfacial engineering for highly efficient quasi-two dimensional organic–inorganic hybrid perovskite light-emitting diodes†

Qing-Wei Liu,^a Shuai Yuan,^a Shuang-Qiao Sun,^a Wei Luo,^a Yi-Jie Zhang,^a
Liang-Sheng Liao ^{ab} and Man-Keung Fung ^{*ab}

Metal halide-based perovskites are regarded as promising candidates for light-emitting diodes (LEDs) owing to their high color purity, tunable bandgap and solution processability. However, poor active-layer morphology and non-radiative charge recombination are still the main obstacles for practical use in displays and lighting. Here, we report a facile method to achieve high-performance green emitting perovskite light-emitting diodes (PeLEDs) by inserting an interface buffer layer (BL) based on an amphipathic conjugated molecule, betaine. We show evidence that the betaine layer controls the grain size of the perovskite and hence increases the crystalline nucleation sites, which ultimately leads to a high photoluminescence quantum yield (PLQY) and a device with an external quantum efficiency (EQE) of 11.1%. In addition, the current leakage is significantly reduced due to the high quality crystallization of the thin film. These results indicate that the interface BL is an effective strategy to boost the efficiency of PeLEDs.

Received 23rd December 2018,
Accepted 19th February 2019

DOI: 10.1039/c8tc06490c

rsc.li/materials-c

Introduction

Perovskite-based materials have been attracting enormous attention in the optoelectronics communities since they can be applied for a wide variety of devices such as perovskite solar cells, light amplifiers and photo detectors.^{1–5} It should be noted that due to their high color purity, easily tunable emission wavelength, facile low-cost solution processing and narrow emitting linewidth, this kind of material has great potential for display and lighting applications.^{6–10} During the past several years, significant progress has been made in green and red-emitting organic electroluminescent devices, which show maximum external quantum efficiencies (EQEs) of more than 20%.^{11–13} To fulfil the application of perovskite light-emitting diodes (PeLED), perovskite-based materials must at least have a high photoluminescence quantum yield (PLQY) and extremely smooth film formation. Simultaneously, the design of a device structure with efficient carrier transport and injection, good matching of energy level alignment, and a reduced exciton quenching effect between the emitting layer and adjacent functional layers also plays a vital

role in acquiring efficient PeLEDs.^{13–16} For traditional organic LEDs, PEDOT:PSS is widely utilized as a hole-injecting layer or a hole-transporting layer (HTL).^{12,17} However, a number of drawbacks, such as acidic, aqueous properties, pose a significant threat to the long-term stability of the devices. Moreover, the mismatched work function not only hardly forms a cascade energy alignment between the anode and the perovskite active layer, but also induces severe exciton quenching, leading to low device efficiency. P-Type polymeric semiconductors with a large band gap such as poly(9-vinylcarbazole) (PVK) or poly[bis(4-phenyl)(4-butylphenyl)amine] (poly-TPD) possess a better energy level match and injection property, and were successfully utilized in quantum-dot LEDs (QLEDs) and PeLEDs.^{18,19} However, one of the challenges of these polymers is the non-ideal wetting surface for the overlying perovskite precursor due to their poor compatibility with polar solutions. This constantly results in inferior surficial coverage with pinholes and higher roughness. Traditional post treatment methods such as oxygen plasma and ultraviolet ozone may chemically destroy the surface of organic materials to a certain extent, causing devices to have a higher turn-on voltage.^{20–23} In this regard, a surface modification that facilitates better interface formation between the HTL and the perovskite active layer is imperative.

Herein, we insert betaine, an interface buffer layer (BL), between the HTL and the perovskite emitting film, which can control the surface wetting properties and increase the number of crystalline nucleation sites, leading to uniform film formation and a confined grain size. Due to the confinement of

^a Jiangsu Key Laboratory for Carbon-Based Functional Materials & Devices, Institute of Functional Nano & Soft Materials (FUNSOM), Soochow University, Suzhou, Jiangsu 215123, China. E-mail: mkfung@suda.edu.cn

^b Institute of Organic Optoelectronics, Jiangsu Industrial Technology Research Institute (JITRI), 1198 Fenuh Dadao, Wujiang, Suzhou, Jiangsu, 215211, P. R. China

† Electronic supplementary information (ESI) available. See DOI: 10.1039/c8tc06490c

the grain size, the perovskite film deposited on the stacked layers of PEDOT:PSS/HTL/BL shows a high exciton binding energy (E_b) of 84.5 meV and a high PLQY. By combining all the advantages of using betaine as the BL, the corresponding PeLEDs exhibit a dramatic enhancement in the current efficiency and EQE.

Results and discussion

The contact angles of the perovskite precursor on different polymeric HTLs, as shown in the top row of Fig. 1, are 56° , 52° and 50° for TFB, PVK and poly-TPD, respectively. The contact angle represents the wetting ability of different substrate surfaces for the perovskite precursor.^{24–26} Here, a modification layer of betaine (an amphipathic molecule) which can improve the wettability of perovskite on polymer films is inserted between the HTL and the active layer. The molecular structure of betaine is shown in Fig. S1 (ESI[†]). As shown in the bottom row of Fig. 1, the contact angle of the perovskite precursor on the various HTLs diminishes significantly.

Fig. 2a shows the contact angle of a perovskite precursor dissolved in dimethyl sulfoxide (DMSO) on PVK, which is about 56° . This indicates poor wettability which in turn leads to fewer nucleation sites and a larger grain size during film formation, as shown in Fig. 2e. Then, we inserted 1 mg ml^{-1} of betaine in isopropanol (spinning speed = 5000 rpm) as a surface modifier between the HTL and the perovskite active layer to improve the wettability of the perovskite precursor on the PVK film. The contact angle decreased markedly to 28° . As the concentration

of betaine was further increased from 5 mg ml^{-1} to 10 mg ml^{-1} , the contact angle decreased continuously to an extremely low value of 11° .

We speculate that there had to be a relationship between the wetting properties and the number of nucleation sites, in which the increased number of nucleation sites is the key criterion for the enhancement of the PLQY and device efficiency. Also, it is commonly believed that a smaller grain size means a better recombination of carriers.²⁵ The effect on how the grain nucleates exerted by the surface tension force can be realized by comparing the grain size of CsPbBr₃ films with different betaine-treated films, and the results are shown in the scanning electron microscopy (SEM) images of Fig. 2e–h. It can be noted that the grain size of CsPbBr₃ on bare PVK is much larger than that of the films modified by different concentrations of betaine. The grain size of CsPbBr₃ grown on bare PVK was around 200 nm, while that grown on PVK modified by 1 mg ml^{-1} of betaine decreased obviously. Furthermore, the perovskite film on bare PVK shows discontinuous grains with many pinholes, which may cause electric shunt paths. This phenomenon is frequently observed in perovskite films fabricated by a one-step spin-coating method.^{27,28} It has been reported that the addition of long-chain ammonium groups strongly improves the crystallization process of perovskite films.^{25,29} Therefore, atomic force microscopy (AFM) was utilized to investigate the surface morphology of CsPbBr₃ on PVK with or without betaine. Fig. 2i–l show the AFM images of perovskite films prepared with different concentrations of betaine, from 0 mg ml^{-1} to 10 mg ml^{-1} . Pristine perovskite has a relatively bumpy surface with a root-mean-square (RMS) roughness of 4.3 nm. When the concentration of betaine was 1 mg ml^{-1} , the perovskite film exhibited a smaller grain size and a reduced surface roughness. When the betaine concentration further increases to 10 mg ml^{-1} , the grain size continues to significantly decrease and the RMS roughness reduces to 0.8 nm, which is beneficial to decrease the leakage current.

From the above, it is clearly shown that with betaine modification we could obtain a highly continuous perovskite film with more uniform coverage, thanks to the amphipathic nature of betaine.

The structures and compositions of these CsPbBr₃ films were characterized by X-ray diffraction (XRD), as shown in Fig. 3a. The diffraction patterns of these CsPbBr₃ thin films match well with single crystal perovskite. The dominant and characteristic diffraction peaks at 15.16° , 21.52° , 30.63° , 37.58°

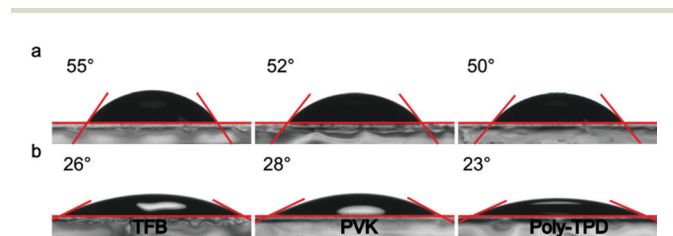


Fig. 1 Contact angles of a perovskite precursor on various HTLs (from left to right: TFB, PVK and poly-TPD) without betaine modification (upper) and with 1 mg ml^{-1} of betaine modification (bottom).

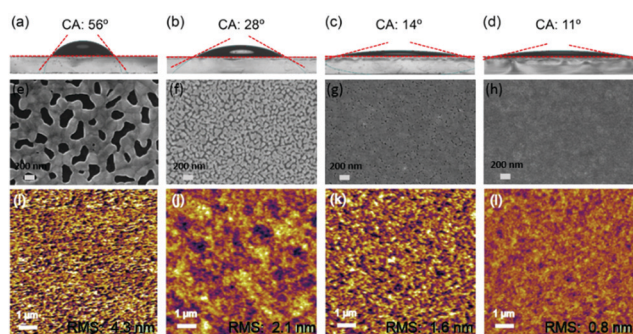


Fig. 2 (a–d) Contact angles of a perovskite precursor with various concentrations of betaine (from left to right: 0, 1, 5 and 10 mg ml^{-1}). (e–h) SEM images and (i–l) AFM topography images of the perovskite films modified with different betaine concentrations.

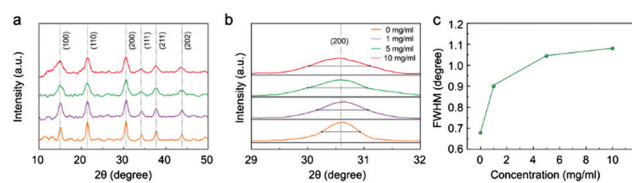


Fig. 3 (a) XRD patterns of perovskites modified with different concentrations of betaine, and (b and c) full-width-at-half-maximum (FWHM) of the (200) peaks as a function of betaine concentration.

and 43.52° can be assigned to the diffraction from the (100), (110), (200), (211) and (202) planes of crystalline CsPbBr_3 , respectively. In addition, there is no significant change in the diffraction peak ratio, indicating that the modification layer does not alter the crystal orientation. However, as seen in Fig. 3b and c, the FWHM of the diffraction peaks broadens with increasing betaine concentration, and the CsPbBr_3 film modified with 10 mg ml^{-1} of betaine shows the widest FWHM of 1.08° , implying that this film has the smallest grain size, which is consistent with the SEM results.

To further investigate the optical properties of CsPbBr_3 films, the CsPbBr_3 film steady-state PL spectra were obtained under continuous 380 nm UV excitation with a calibrated light intensity at room temperature (RT). The inset of Fig. 4a shows the PL spectrum of the CsPbBr_3 thin film. Its characteristic is a highly symmetric emission peak at 512 nm with a narrow FWHM of 22 nm. Furthermore, the absolute PLQY of the CsPbBr_3 films was measured using a fluorescence spectrometer with an excitation wavelength of 400 nm. The PLQY of the perovskite films fabricated by spin-coating CsPbBr_3 onto the betaine modified film was measured, and the value was found to be within the range of 32% to 48%. Moreover, the PLQY of the perovskite film directly spin-coated onto the bare PVK was also measured for comparison, and a relatively low value of 6% was obtained (Fig. 4a). From this phenomenon we speculate that the increased photoluminescence yield for the betaine modified films is attributed to the increase of exciton binding energy and the electron-hole recombination probability that has arisen from the smaller CsPbBr_3 grain size.^{10,30,31}

In order to further explore the photoinduced excitations in CsPbBr_3 films, the PL decay lifetime is measured from the time-correlated single photon counting (TCSPC) spectra shown in

Fig. 4b. The PL decay from the CsPbBr_3 films can be fitted to a biexponential decay, exhibiting a weighted-average lifetime (τ) of $\sim 20 \text{ ns}$ for the pristine film, which is much shorter than those of CsPbBr_3 modified with 5 mg ml^{-1} betaine, *i.e.* $\sim 80 \text{ ns}$.

To obtain more insight into the photoinduced excitations and the exciton binding energy of CsPbBr_3 which affects the efficiency of charge transfer and exciton dissociation probability, temperature-dependent PL measurements which gauge the exciton binding energy were carried out with the temperature ranging from 300 K (RT) to 80 K (Fig. 4c). The E_b of the CsPbBr_3 films can be obtained by the following equation:^{32,33}

$$I(T) = \frac{I_0}{1 + A \exp\left(-\frac{E_b}{K_B T}\right)} \quad (1)$$

Here, I_0 represents the emission intensity at 0 K, A is a proportional constant, E_b is the exciton binding energy and K_B is the Boltzmann constant. Upon fitting the curves, the exciton binding energies E_b are 40.5, 60.5, 84.5 and 104 meV for pristine CsPbBr_3 , CsPbBr_3 -1 mg ml^{-1} betaine, CsPbBr_3 -5 mg ml^{-1} betaine, and CsPbBr_3 -10 mg ml^{-1} betaine films, respectively. As presented in Fig. 4d, CsPbBr_3 -10 mg ml^{-1} betaine film displays the highest E_b , which is consistent with the above result that this film has the strongest PLQY intensity.

All of these results clearly indicate that a smaller grain size of perovskite would lead to a longer lifetime (τ) of 80 ns and a relatively high PLQY. A higher PLQY is expected to contribute to the significant increase in the E_b and electron-hole recombination.^{34,35} This may also be ascribed to the passivation of the perovskite film due to hydrophilic betaine.

To further investigate the above inference and ratiocination, and the rationality of applying the modification layer for efficient light emission, green perovskite LED devices with a multilayer structure consisting of indium tin oxide (ITO), PEDOT:PSS, PVK, betaine (different concentrations), CsPbBr_3 , 1,3,5-tris(1-phenyl-1H-benzimidazol-2-yl)benzene (TPBi), lithium 8-hydroxyquinolate (LiQ) and Al were fabricated, as shown in Fig. 5a. The corresponding energy levels of the materials are shown in Fig. S2 (ESI[†]). The thicknesses of the emitting layer and the betaine modification layer with different concentrations are 50 and 7 nm, respectively, which were measured using an ellipsometer. The device cross-section is illustrated in the scanning electron microscopy (SEM) micrograph shown in Fig. 5b, from which an orderly multilayer configuration can be observed. Fig. 5c depicts the luminescence-current density (L - J) curves of CsPbBr_3 modified by 5 mg ml^{-1} betaine. The turn-on voltage (tested at 1 cd m^{-2}) of the PeLED is about 3.8 V. With a high-quality perovskite film, the highest luminescence of 18560 cd m^{-2} was achieved at a current density of 115 mA cm^{-2} . Fig. 5d displays the voltage-current density characteristics of devices based on pristine CsPbBr_3 and CsPbBr_3 treated with 1/5/10 mg ml^{-1} betaine. Furthermore, the device modified by betaine exhibited an extremely low leakage current of below $10^{-4} \text{ mA cm}^{-2}$, as shown in Fig. S3 (ESI[†]). In addition, the luminance yield and EQE of the devices as a function of current density are plotted in Fig. 5e and f, respectively. A device

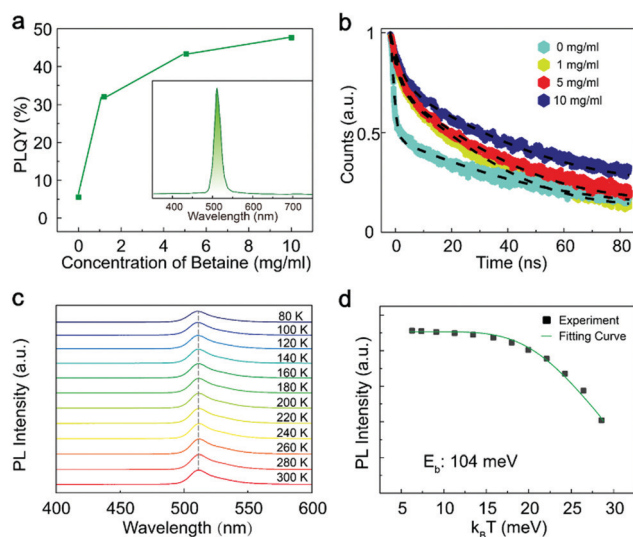


Fig. 4 (a) PLQY of perovskite, as a function of betaine concentration. (b) TCSPC spectra of pristine CsPbBr_3 , CsPbBr_3 -1 mg ml^{-1} betaine, CsPbBr_3 -5 mg ml^{-1} betaine and CsPbBr_3 -10 mg ml^{-1} betaine films. (c) Temperature-dependent PL spectra of the CsPbBr_3 film recorded at 80 K to 300 K. (d) The relevant integration of PL intensity based on the CsPbBr_3 -10 mg ml^{-1} betaine film.

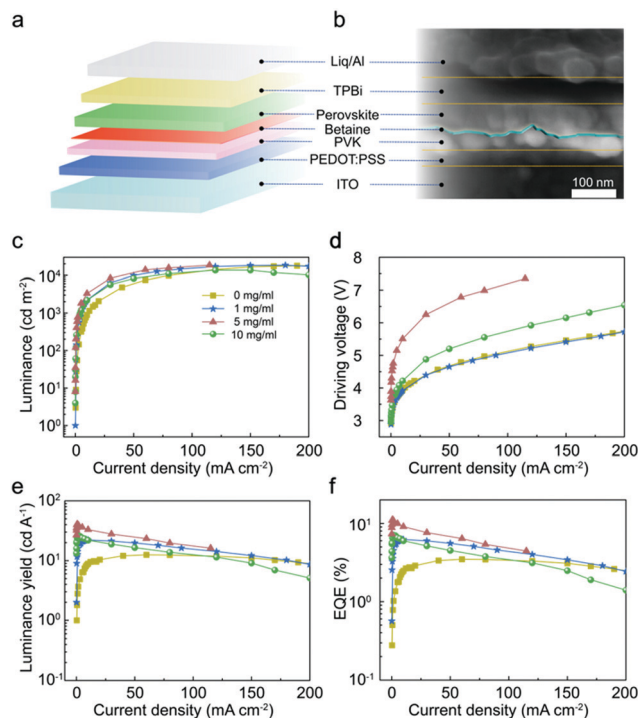


Fig. 5 (a) Schematic diagram of device structure: ITO/PEDOT:PSS/PVK/perovskite/TPBi/Liq/Al. (b) Cross-sectional SEM image of the PeLED. (c) Luminous yield versus current density of the PeLED. (d) Driving voltage of the PeLED as a function of current density. (e) Luminance yield versus current density. (f) EQE of the PeLED.

fabricated with pristine CsPbBr₃ shows the lowest current efficiency and EQE of 12.48 cd A⁻¹ and 3.48%, respectively. In contrast, a peak current efficiency and a maximum EQE of 40.4 cd A⁻¹ and 11.11% are achieved when the 5 mg ml⁻¹ betaine film is used as the modification layer. Although both the 5 mg ml⁻¹ and 10 mg ml⁻¹ betaine modified perovskite films have similar physical and optical properties, the efficiency of the PeLED treated with 10 mg ml⁻¹ betaine is lower than that modified with 5 mg ml⁻¹ betaine. This is because betaine at such a high concentration may have a relatively poor conductivity. To verify the repeatability of CsPbBr₃ based PeLEDs treated with 5 mg ml⁻¹ betaine, a histogram of EQEs with an average value of 9.5% for 32 devices is shown in Fig. S4 (ESI†).

Fig. 6a shows the EL spectra of CsPbBr₃-5 mg ml⁻¹ betaine devices under different biases, which exhibit a single and well-defined emission peak at 516 nm with the emission intensity increasing gradually with the voltage. The EL spectra agree well with the previously measured PL spectra. In addition, the FWHM of the detected EL spectrum at 7.3 V is about 23 nm. There is no manifestation of broadening behaviour with the applied voltage. This narrow EL emission means that the device has a high color purity. The inset of Fig. 6a shows the device photo (0.1 cm²) driven at 6.4 V. The color of the device is highly saturated in the deep green region which corresponds to a Commission International de Eclairage (CIE) (x,y) of (0.10,0.76), as shown in Fig. 6b. The angular emission intensity of the device follows a Lambertian profile, which is shown in Fig. S5 (ESI†).

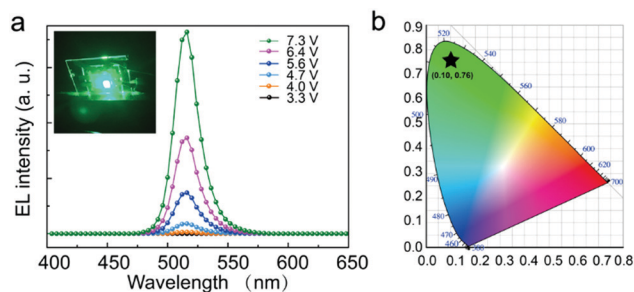


Fig. 6 (a) EL spectra of the PeLED under different applied voltages, together with a typical emission photograph of the PeLED with an active area of 0.1 cm² (at 6.4 V). (b) CIE coordinates of the PeLED under an applied voltage of 6.4 V.

Experimental section

Materials

PbBr₂, CsBr, DMSO (anhydrous, 99.9%) and PVK were purchased from Sigma-Aldrich. TPBi (99.9%) and Liq were purchased from Xi'an Polymer Light Technology Corp. PEDOT:PSS (Clevis P VP Al 4083) was purchased from Heraeus. All the materials were used as purchased without any purification.

Preparation of perovskite solutions for device fabrication

A hybrid halide precursor solution for the perovskite film was prepared by dissolving CsBr, PbBr₂ and PEABr in DMSO at a molar ratio of 1.1:1:0.4, here PbBr₂ is fixed at 0.3 M. The solution was then stirred for 5 h and filtered through polytetrafluoroethylene filters (0.45 μm) before use.

Patterned ITO glass substrates were sequentially cleaned with ethanol and deionized (DI) water. They were then subjected to UV-ozone treatment for 10 min. The HTL was prepared by spin coating PEDOT:PSS (AI 4083) at 5000 rpm onto the ITO substrate, which was then dried at 150 °C for 30 min to remove the remaining water. The substrates were then transferred into a glove box for further processing. The PVK layer was spin coated onto the PEDOT:PSS film with a 8 mg ml⁻¹ concentration dissolved in chlorobenzene at 4000 rpm. Then the substrates were subjected to annealing treatment for 10 min on a hot plate at 120 °C. After this step, the perovskite film with or without the betaine layer was deposited on top of PVK by repeating the spin-coating procedure mentioned above, followed by annealing at 85 °C for 8 min. Finally, TPBi (45 nm), Liq (2 nm) and Al (120 nm) layers were deposited on top of the perovskite EML in a thermal evaporation chamber with a vacuum pressure below 4 × 10⁻⁴ Pa. The final devices possessed 4 emitting elements each with an active area of 0.1 cm².

Film characterization and device measurements

The contact angle data were collected by a DataPhysics OCA. SEM images of the layers were obtained on a Carl Zeiss Supra 55. AFM measurements were conducted using a Cypher-S atomic force microscope. XRD spectra were obtained on an X-ray diffractometer with a Cu Kα source (PANalytical B.V. Empyrean). PL decay lifetimes were obtained on a fluorescence

spectrophotometer (HORIB-FM-2015). Photoluminescence spectra were recorded on a FluoroMax-4 spectrophotometer (Horiba Scientific, USA). The temperature-dependent measurements were performed using a closed-cycle nitrogen cryostat. Excitation power intensity dependent PL was carried out by employing a neutral filter and the excitation power density was monitored by a Thorlabs PM100D 4" LCD power meter.

The EL spectra and electrical output characteristics were obtained under ambient conditions using a Keithley 2400 and a Photo Research spectrometer PR650. The devices were swept from zero bias to forward bias.

Conclusions

In summary, we have proposed a facile method by introducing a betaine modification layer to improve the crystallinity of the perovskite layer and obtain a pinhole-free perovskite film. Benefitting from the small grain size and high E_b , the CsPbBr₃-based PeLED with a 5 mg ml⁻¹ doped betaine modification layer exhibited a high current efficiency of 40.4 cd A⁻¹ and a maximum luminance of 18 560 cd m⁻². An EQE of 11.1% was also achieved at a current density of 0.5 mA cm⁻². We have proven that a smooth morphology, a high exciton binding energy and an increased electron-hole recombination associated with a smaller CsPbBr₃ grain size are crucial factors that would determine the device performance. Our results confirm that incorporation of an interface buffer layer of betaine is an effective means to boost the efficiencies of PeLEDs.

Conflicts of interest

There are no conflicts to declare.

Acknowledgements

Q. W. Liu and S. Yuan contributed equally to this work. The authors acknowledge financial support from the National Key R&D Program of China (No. 2016YFB0400703), the National Natural Science Foundation of China (61475106 and 61875144), the Natural Science Foundation of Jiangsu Province (BK20151264), the Collaborative Innovation Center of Suzhou Nano Science and Technology (NANO-CIC), the 111 project, and the Priority Academic Program Development of Jiangsu Higher Education Institutions.

Notes and references

- H. P. Zhou, Q. Chen, G. Li, S. Luo, T. B. Song, H. S. Duan, Z. R. Hong, J. B. You, Y. S. Liu and Y. Yang, *Science*, 2014, **345**, 542–546.
- A. Kojima, K. Teshima, Y. Shirai and T. Miyasaka, *J. Am. Chem. Soc.*, 2009, **131**, 6050.
- Z. K. Tan, R. S. Moggaddam, M. L. Lai, P. Docampo, R. Higler, F. Deschler, M. Price, A. Sadhanala, L. M. Pazos and D. Credgington, *Nat. Nanotechnol.*, 2014, **9**, 687.
- A. Perulli, A. Balena, M. Fernandez, G. Nedelcu, A. Creti, M. V. Kovalenko, M. Lomascolo and M. Anni, *Appl. Phys. Lett.*, 2018, **112**, 171904.
- A. Balena, A. Perulli, M. Fernandez, M. L. De Giorgi, G. Nedelcu, M. V. Kovalenko and M. Anni, *J. Phys. Chem. C*, 2018, **122**, 5813–5819.
- F. Zhang, H. Zhong, C. Chen, X. G. Wu, X. Hu, H. Huang, J. Han, B. Zou and Y. Dong, *ACS Nano*, 2015, **9**, 4533.
- M. J. Yuan, L. N. Quan, R. Comin, G. Walters, R. Sabatini, O. Voznyy, S. Hoogland, Y. B. Zhao, E. M. Beauregard, P. Kanjanaboos, Z. H. Lu, D. H. Kim and E. H. Sargent, *Nat. Nanotechnol.*, 2016, **11**, 872.
- B. Saparov and D. B. Mitzi, *Chem. Rev.*, 2016, **116**, 4558.
- S. Koch, M. Kira, G. Khitrova and n. Gibbs, *Nat. Mater.*, 2006, **5**, 523.
- H. Cho, S. H. Jeong, M. H. Park, Y. H. Kim, C. Wolf, C. L. Lee, J. H. Heo, A. Sadhanala, N. Myoung and S. Yoo, *Science*, 2015, **350**, 1222.
- B. D. Zhao, S. Bai, V. Kim, R. Lamboll, R. Shivanna, F. Auras, J. M. Richter, L. Yang, L. J. Dai, M. Alsari, X. J. She, L. S. Liang, J. B. Zhang, S. Lilliu, P. Gao, H. J. Snaith, J. P. Wang, N. C. Greenham, R. H. Friend and D. W. Di, *Nat. Photonics*, 2018, **12**, 783.
- K. B. Lin, J. Xing, L. N. Quan, F. P. G. de Arquer, X. W. Gong, J. X. Lu, L. Q. Xie, W. J. Zhao, D. Zhang, C. Z. Yan, W. Q. Li, X. Y. Liu, Y. Lu, J. Kirman, E. H. Sargent, Q. H. Xiong and Z. H. Wei, *Nature*, 2018, **562**, 245.
- Y. Cao, N. N. Wang, H. Tian, J. S. Guo, Y. Q. Wei, H. Chen, Y. F. Miao, W. Zou, K. Pan, Y. R. He, H. Cao, Y. Ke, M. M. Xu, Y. Wang, M. Yang, K. Du, Z. W. Fu, D. C. Kong, D. X. Dai, Y. Z. Jin, G. Q. Li, H. Li, Q. M. Peng, J. P. Wang and W. Huang, *Nature*, 2018, **562**, 249.
- J. Xing, F. Yan, Y. W. Zhao, S. Chen, H. K. Yu, Q. Zhang, R. G. Zeng, H. V. Demir, X. W. Sun, A. Huan and Q. H. Xiong, *ACS Nano*, 2016, **10**, 6623–6630.
- Y. C. Ling, Z. Yuan, Y. Tian, X. Wang, J. C. Wang, Y. Xin, K. Hanson, B. W. Ma and H. W. Gao, *Adv. Mater.*, 2016, **28**, 305–311.
- J. W. Lee, Y. J. Choi, J. M. Yang, S. Ham, S. K. Jeon, J. Y. Lee, Y. H. Song, E. K. Ji, D. H. Yoon, S. Seo, H. Shin, G. S. Han, H. S. Jung, D. Kim and N. G. Park, *ACS Nano*, 2017, **11**, 3311.
- N. Yantara, S. Bhaumik, F. Yan, D. Sabba, H. A. Dewi, N. Mathews, P. P. Boix, H. V. Demir and S. Mhaisalkar, *J. Phys. Chem. Lett.*, 2015, **6**, 4360–4364.
- Q. Sun, Y. A. Wang, L. S. Li, D. Y. Wang, T. Zhu, J. Xu, C. H. Yang and Y. F. Li, *Nat. Photonics*, 2007, **1**, 717–722.
- T. Chiba, Y. Hayashi, H. Ebe, K. Hoshi, J. Sato, S. Sato, Y. J. Pu, S. Ohisa and J. Kido, *Nat. Photonics*, 2018, **12**, 681.
- X. Xiao, C. Bao, Y. Fang, S. Tang, Y. Liu, Y. Deng, X. Zheng, Y. Gao, X. C. Zeng and J. Huang, *Adv. Mater.*, 2018, **30**, 1705176.
- W. Wang, Y. Li, X. Wang, Y. Lv, S. Wang, K. Wang, Y. Shi, L. Xiao, Z. Chen and Q. Gong, *Phys. Rev. B: Condens. Matter Mater. Phys.*, 2016, **94**, 140302.
- C. L. Wang, D. W. Zhao, C. R. Grice, W. Q. Liao, Y. Yu, A. Cimaroli, N. Shrestha, P. J. Roland, J. Chen, Z. H. Yu,

- P. Liu, N. Cheng, R. J. Ellingson, X. Z. Zhao and Y. F. Yan, *J. Mater. Chem. A*, 2016, **4**, 12080–12087.
- 23 O. Vybornyi, S. Yakunin and M. V. Kovalenko, *Nanoscale*, 2016, **8**, 6278–6283.
- 24 F. Hao, C. C. Stoumpos, P. J. Guo, N. J. Zhou, T. J. Marks, R. P. H. Chang and M. G. Kanatzidis, *J. Am. Chem. Soc.*, 2015, **137**, 11445–11452.
- 25 G. Rothenberger, J. Moser, M. Gratzel, N. Serpone and D. K. Sharma, *J. Am. Chem. Soc.*, 1985, **107**, 8054–8059.
- 26 M. Xiao, F. Huang, W. Huang, Y. Dkhissi, Y. Zhu, J. Etheridge, A. Gray-Weale, U. Bach, Y. B. Cheng and L. J. A. C. I. E. Spiccia, *Angew. Chem.*, 2014, **53**, 9898–9903.
- 27 Z. B. Wang, Z. Luo, C. Y. Zhao, Q. Guo, Y. P. Wang, F. Z. Wang, X. M. Bian, A. Alsaedi, T. Hayat and Z. A. Tan, *J. Phys. Chem. C*, 2017, **121**, 28132–28138.
- 28 Z. H. Wei, A. Perumal, R. Su, S. Sushant, J. Xing, Q. Zhang, S. T. Tan, H. V. Demir and Q. H. Xiong, *Nanoscale*, 2016, **8**, 18021–18026.
- 29 S. Yuan, Z. K. Wang, M. P. Zhuo, Q. S. Tian, Y. Jin and L. S. Liao, *ACS Nano*, 2018, **12**, 9541–9548.
- 30 Y. H. Kim, H. Cho, J. H. Heo, T. S. Kim, N. Myoung, C. L. Lee, S. H. Im and T. W. Lee, *Adv. Mater.*, 2015, **27**, 1248.
- 31 N. Yantara, S. Bhaumik, F. Yan, D. Sabba, H. A. Dewi, N. Mathews, P. P. Boix, H. V. Demir and S. Mhaisalkar, *J. Phys. Chem. Lett.*, 2015, **6**, 4360.
- 32 L. Zhang, X. Yang, Q. Jiang, P. Wang, Z. Yin, X. Zhang, H. Tan, Y. M. Yang, M. Wei and B. R. Sutherland, *Nat. Commun.*, 2017, **8**, 15640.
- 33 Z. Chen, C. Yu, K. Shum, J. J. Wang, W. Pfenninger, N. Vockic, J. Midgley and J. T. Kenney, *J. Lumin.*, 2012, **132**, 345–349.
- 34 T. Chiba, K. Hoshi, Y. J. Pu, Y. Takeda, Y. Hayashi, S. Ohisa, S. Kawata and J. Kido, *ACS Appl. Mater. Interfaces*, 2017, **9**, 18054–18060.
- 35 S. D. Stranks, V. M. Burlakov, T. Leijtens, J. M. Ball, A. Goriely and H. J. Snaith, *Phys. Rev. Appl.*, 2014, **2**, 034007.